

Polyhydroxybutyrate-Based Nanocomposites with Cellulose Nanocrystals and Bacterial Cellulose

I. T. Seoane¹ · P. Cerrutti² · A. Vazquez² · L. B. Manfredi¹ · V. P. Cyras¹

Published online: 24 September 2016
© Springer Science+Business Media New York 2016

Abstract Polyhydroxybutyrate (PHB) films nanoreinforced with hydrolyzed cellulose nanocrystals (CNC) and bacterial cellulose (BC) were prepared by solvent casting. The influence of different cellulose nanoparticles content (2, 4 and 6 wt% of CNC and 2 wt% of BC) on the PHB properties was studied. CNC nanocomposites presented good dispersion of the nanocrystals, improving transparency, mechanical and barrier properties of the PHB films. On the other hand, reduced thermal stability and mechanical properties were yielded by BC addition due to the intrinsic lower degradation temperature and higher length of the BC nanofibrils compared to CNC. Nanocomposites performance variation is mainly caused by the marked difference in nanoparticles structure. It was demonstrated that PHB–CNC films exhibited higher performance enhancement without detrimental effect of the pristine PHB properties.

Keywords Polyhydroxybutyrate · Cellulose nanoparticles · Nanocomposites

Introduction

Due to the growing environmental alertness about the reliable availability of petrochemicals in the future, efforts are being made by researchers to design and produce biodegradable polymers and composites based on renewable natural resources. These biodegradable materials will be important in so far as its properties being suitable for a wide range of applications.

Polyhydroxybutyrate (PHB) is a microbial storage polymer, accumulated by a variety of bacteria as a reserve of carbon and energy, under conditions of nutrient stress. PHB is a biodegradable material which can be completely degraded and assimilated by a vast range of microorganisms into innocuous, naturally going on molecules [1, 2]. Additionally, PHB is a thermoplastic polyester which can be extruded and molded on conventional processing equipment [3]. Moreover, due to its natural origin, PHB has stereochemical regularity and their chains are completely linear, which implies that this polymer is completely isotactic and capable of crystallizing, with a crystallinity around 60 %. Due to its high crystallinity and hydrophobic character the PHB has excellent barrier properties to use on films [4]. However, PHB presents some problems, such as high cost, slow crystallization rate, high degree of crystallinity, a narrow window for the processing conditions, which could be resolved [5–8]. In general, the development of nanocomposites promises to expand the use of biodegradable films, improving matrix properties [9–11].

Numerous important studies over the last decades have shown that cellulose nanoparticles could be used as fillers to improve mechanical and barrier properties of biocomposites [12, 13]. Cellulose is the most abundant biomass material in nature [12, 13], and cellulose nanocrystals (CNC) can be obtained by strong acid hydrolysis of

✉ V. P. Cyras
VPCYRAS@FL.MDP.EDU.AR

¹ Ecomateriales, Facultad de Ingeniería, Instituto de Investigaciones en Ciencia y Tecnología de Materiales (INTEMA), UNMdP, CONICET, J.B. Justo 4302, 7600 Mar del Plata, Argentina

² Fac. de Ingeniería, Instituto de Tecnología en Polímeros y Nanotecnología (ITPN), UBA, CONICET, Las Heras 2214, 1127 Buenos Aires, Argentina

cellulose microfibrils, or microbially produced. Important structural features and properties of bacterial cellulose (BC) are purity, degree of polymerization (up to 8000), crystallinity and mechanical stability. So, nanosized cellulose particles are promising candidates for bionanocomposites preparation, due to their abundance, high strength and stiffness, low weight and biodegradability.

The use of cellulose nanoparticles derived from renewable resources as a reinforcing phase in polymeric matrix composites provides a reduced environmental impact, because it will help to reduce the packaging waste associated with processed foods and it will support the preservation of fresh foods, extending their shelf life [14]. Such nanocomposites possess very unusual properties [15, 16], very different from their microscale counterparts, and often show improved mechanical and thermal stability. PHB-nanoparticle composites could be obtained by means of solvent casting with polar solvents and dried methods, as impregnation and extrusion [12]. Nanocomposite obtaining process is important because it determines the material final properties. Cao et al. [17] had found that the presence of CNC agglomerations in cement pastes depends on dispersion process and it is significant for performance improvement. In addition, dispersion and specific area of the nanoparticles have an important role on final properties, because they influence particle–matrix and particle–particle interactions [18]. All natural fibers are hydrophilic in nature due to the presence of large amounts of hydroxyl groups which often results in poor compatibility with hydrophobic polymer matrices then lowering mechanical properties of the composite [19].

It was reported the use of various biodegradable polymers as matrices for nanocomposites reinforced with nanocellulose [12]. However, in the literature there are few studies on PHB-based nanocomposites with CNC or BC, where matrix performance is improved [11, 20]. PHB/CNC nanocomposites present significant increase in the thermal stability with low CNC concentrations, but with no significant change in the degradation mechanism [20]. In the case of PHB/BC composites, cellulose microfibrils are usually soaked in a suspension of PHB and when the solvent is evaporated, PHB is incorporated into the cellulose microfibrils.

In the current work, the structure-properties relationship of nanocomposites based on PHB with different cellulose nanoparticles types (CNC and BC) was studied. The same nanocomposite obtaining process for both nanoparticles was used in order to compare the nanofillers effect on matrix properties. Some particular properties of the materials required to be used in packaging (laminated foils, hygiene, fast food, one-way cups, agricultural foils, etc.), such as mechanical, water vapor exposure and transparency were particularly analyzed. A detail comparison regarding

the final properties of both types of nanocomposites was done.

Experimental

Materials

PHB was kindly supplied by Biocycle[®]. Microcrystalline cellulose (MCC, dimensions of 10–15 μm) was supplied by Sigma–Aldrich (St. Louis, MO, USA). *N,N*-Dimethylformamide (DMF) and Sulphuric acid were from Cicarelli.

Methods

Preparation of Cellulose Nanoparticles

MCC was hydrolyzed in sulphuric acid (64 wt%) at 45 °C for 40 min following the recipe used by Morán et al. [21]. Immediately following the acid hydrolysis, the suspension was diluted with bi-distilled water to quench the reaction. The suspension was dialyzed against water for 10 days and an ultrasonic treatment was performed by means of a tip sonicator (Cole Parmer) for 4 times of 5 min. Finally, CNC were freeze dried by a VirTis benchtop SLC lyophilizer and examined by Scanning Electron Microscope (SEM Carl Zeiss NTS SUPRA 40) and Atomic Force Microscopy (AFM Agilent 5500).

BC used in this work was produced by *Gluconacetobacter xylinus* using non-conventional low-cost carbon sources, such as glycerol remaining from biodiesel production and grape bagasse [22].

Preparation of Nanocomposite Films

Homogeneous solutions of PHB in DMF were prepared by stirring at 116 °C. Different amounts of CNC (2, 4 and 6 wt%) previously ultrasonicated in DMF were added to this solution. After that, the mixes were ultrasonicated. Finally, the solutions were poured into Petri dishes and kept in an oven at 80 °C for 12 h to eliminate solvent by evaporation. The films were stored at room temperature for 15 days to complete PHB crystallization. Nanocomposites with 2 wt% of BC were prepared in the same way but using a homogenizer to promote the dispersion.

Nanocomposite Characterization

Attenuated total reflectance Fourier transform infrared (ATR-FTIR) spectra were acquired with a Mattson Genesis II spectrometer, with a spectral width of 400–4000 cm^{-1} , 32 accumulations, and a 4 cm^{-1} resolution. For comparison purposes, the spectra were normalized with the

intensity of the band near 2933 cm^{-1} , which corresponds to the group CH_2 that is present in all samples.

X-ray Diffraction (XRD) measurements were obtained with $\text{KC}\alpha$ ($\lambda = 1.54\text{ \AA}$) radiation in a Philips PW 1710 X-ray diffractometer system. The X-ray tube was operated at 40 kV and 40 mA, at $2^\circ/\text{min}$ in the 2θ range from 5° to 60° . Crystallinity degree (X_c) was calculated using Eq. 1, that relates amorphous and crystalline areas assessed from the spectra [23]:

$$X_c(\%) = \frac{(\text{Totalarea}) - (\text{Amorphousarea})}{(\text{Totalarea})} \times 100 \quad (1)$$

Differential Scanning Calorimetry (DSC) analyses were carried out using a Perkin Elmer DSC instrument with intracooler for refrigeration under nitrogen atmosphere. The samples were first heated from room temperature to 200°C at a heating rate of $10^\circ\text{C}/\text{min}$ to determine melting temperatures (T_{m1} and T_{m2}), held 1 min at constant temperature and then cooled to -50°C at $10^\circ\text{C}/\text{min}$. Subsequently, the samples were heated to 195°C at $10^\circ\text{C}/\text{min}$ to obtain the glass transition temperature (T_g), crystallization temperature (T_c) and new melting temperatures in that condition. Crystallinity degree of PHB can be determined using the following Eq. (2), which considers the area of melting peaks as the necessary heat to crystals fusion:

$$X_c(\%) = \frac{\Delta H_m}{\Delta H_m^0 \cdot w_{PHB}} \times 100 \quad (2)$$

where ΔH_m is PHB melting enthalpy, ΔH_m^0 is the melting heat associated with pure crystalline PHB (146 J/mol) [24] and w_{PHB} is the weight fraction of PHB in the composite.

Thermogravimetric Analyses (TGA) were performed in a TA Q500. Temperature was raised from room temperature up to 700°C at $10^\circ\text{C}/\text{min}$ heating rate. All runs were carried out under nitrogen atmosphere in order to prevent any thermo-oxidative reaction.

Dynamic Mechanical Analysis (DMA) was executed by means of a RHEOPLUS/32 rheometer. The frequency used was 1 Hz and the heating rate was $5^\circ\text{C}/\text{min}$. Each material was characterized by at least three samples.

Mechanical properties of the composites were determined with an INSTRON 4467 mechanical testing machine. Tensile testing of at least ten bone-shaped specimens per material was carried out using a crosshead rate of $1\text{ mm}/\text{min}$ (ASTM D 1708-93).

Film transparency was studied using rectangular strips directly placed in a UV–visible spectrophotometer test cell. Transmittance spectrum was obtained from 200 to 800 nm in an Agilent 8453 UV–visible spectrophotometer. The thickness of the films used in this analysis was $50\text{ }\mu\text{m}$.

Water vapor permeability tests were conducted using ASTM E 96-00e1. Each film sample was sealed over a circular opening of 0.00177 m^2 in a permeation cell and

was conditioned at 20°C in desiccators before being analyzed. Test cells were placed in a conditioned chamber at 20°C and 64.5 % of relative humidity (RH). Anhydrous CaCl_2 (0 % RH) was placed inside the cell to maintain a humidity gradient across the film. The RH inside the cell was always lower than that outside, and water vapor transport was determined from the weight gain of the permeation cell. When steady state conditions were reached (about 1 day), weight measurements were made over 10 days. Changes in the weight of the cell were recorded as a function of time for all the samples. Water vapor transmission rate (WVTR) is a weight gain and was calculated as the relation between the slope of each curve of weight vs time (g/s), determined by linear regression, and the cell area (m^2). Water vapor permeability (WVP) value was determined applying Eq. 3:

$$WVP\left(\frac{\text{g}}{\text{s} \cdot \text{m} \cdot \text{Pa}}\right) = \frac{WVTR}{S \cdot (R2 - R1)} \cdot d \quad (3)$$

where S is vapor pressure of water at saturation (Pa) at test temperature (20°C), $R1$ is RH inside the permeation cell ($R1 = 0$), $R2$ is RH in the chamber ($R2 = 64.5\%$) and d is film thickness (m). Each WVP reported was the mean value of at least six samples.

Results and Discussion

CNC and BC Characterization

Morphological Characterization

CNC size distribution was determined from AFM and SEM micrographs of at least 100 elements. Figure 1 shows AFM images of CNC. The average diameter and length of cellulose nanoparticles was 3–6 nm and 130–290 nm, respectively. The relative frequencies and Gaussian distributions of each dimension are represented in Fig. 2. Figure 3 shows SEM images of CNC and BC. On the other hand, BC is composed by ribbon-shaped microfibrils that are several micrometers long and they have rectangular cross-sections with widths and thicknesses in the range of 35–70 and 13–24 nm, respectively [22]. This structure is formed during the synthesis due to van der Waals forces and hydrogen bonding of adjacent molecules that promote parallel stacking of multiple cellulose chains forming elementary fibrils that aggregate into larger microfibrils [16].

Fourier Transform Infrared Spectroscopy

FT-IR spectra of MCC, CNC and BC are shown in Fig. 4. These spectra show the characteristic peaks of typical structure of cellulose I, with some minor changes,

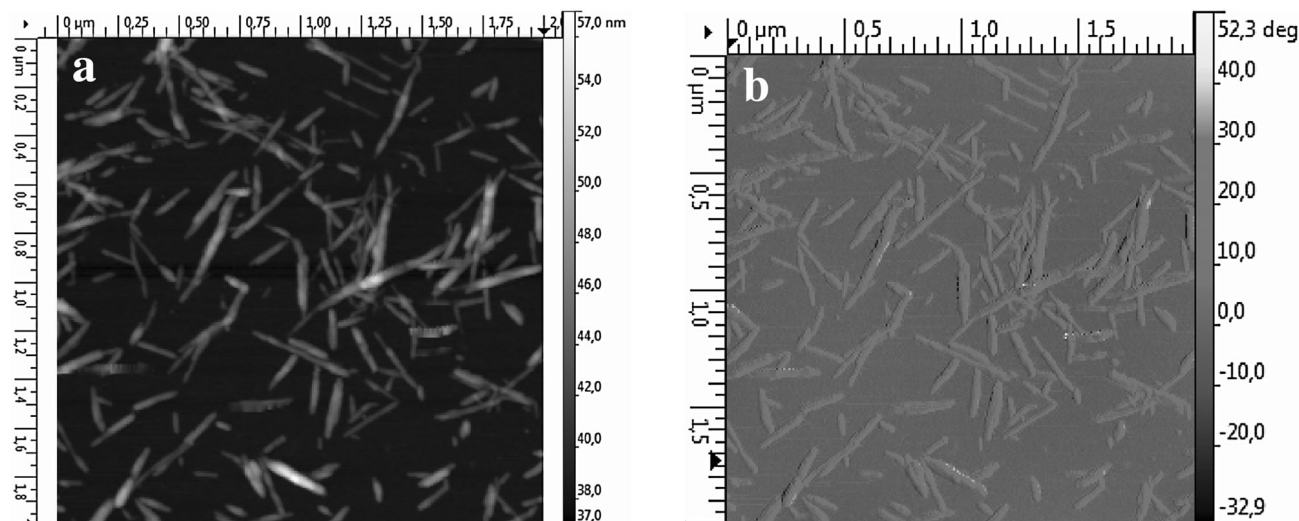


Fig. 1 AFM images of CNC **a** topography and **b** phase

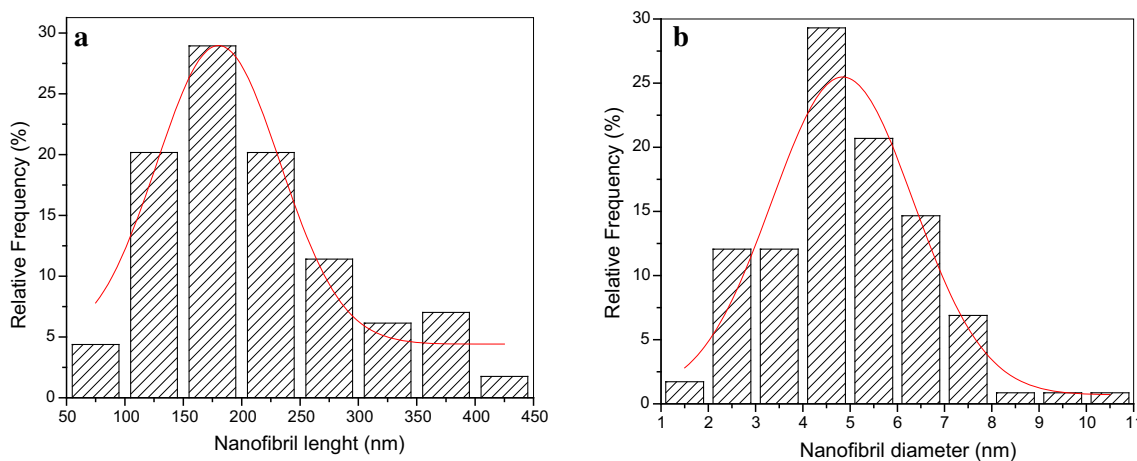


Fig. 2 **a** Length distribution of CNC. **b** Diameter size distribution of CNC

indicating that cellulose kept the same chemical structure. The characteristic bands of cellulose I appeared at 1429 cm^{-1} assigned to CH_2 symmetrical bending, 1105 cm^{-1} assigned to C–O bond stretching and a weak band centered at about 893 cm^{-1} , typical of β -linked glucose polymers.

It was also observed a slightly increase of the CNC absorbance peak at 3350 cm^{-1} respect to MCC spectrum, attributed to hydroxyl groups. During CNC production via acid hydrolysis, amorphous regions of the cellulose are preferentially hydrolyzed, producing nanocrystals [14]. Hydroxyl groups are created from the cellulose glycosidic bond in the cleavage of the microfibrils [25]. On the other hand, BC is characterized by a high polymerization grade, forming a reticulated structure connected by strong hydrogen bonds [22]. This could explain the slightly lower absorbance of –OH band; also this peak could be thinner because of the typical high ordered and pure BC structure.

Additional changes in the band at 1030 and 1109 cm^{-1} could be associated with ether C–O–C and C–O bond stretching, respectively, and the dissimilarities in the bands at 3220 – 3342 cm^{-1} could indicate variations in intermolecular and intramolecular hydrogen bonds between BC and CNC. Finally, the band located at 1635 cm^{-1} is also related to hydrogen bonds of hydroxyl groups of BC [21, 26]. IR absorption bands at 1370 cm^{-1} (CH_2 bending) and 1430 cm^{-1} (symmetric CH_2 bending vibrations) are indicative of the crystallinity of BC.

X-ray Diffraction Analyses

CNC and BC are crystalline as it can be seen from XRD analyses, in Fig. 5. The XRD patterns show that the major intensity peak is located at 22.7° of 2θ value, which is related to the crystalline structure of cellulose I [27]. Also, the peaks observed at 14 – 16° and 34.4° are characteristic

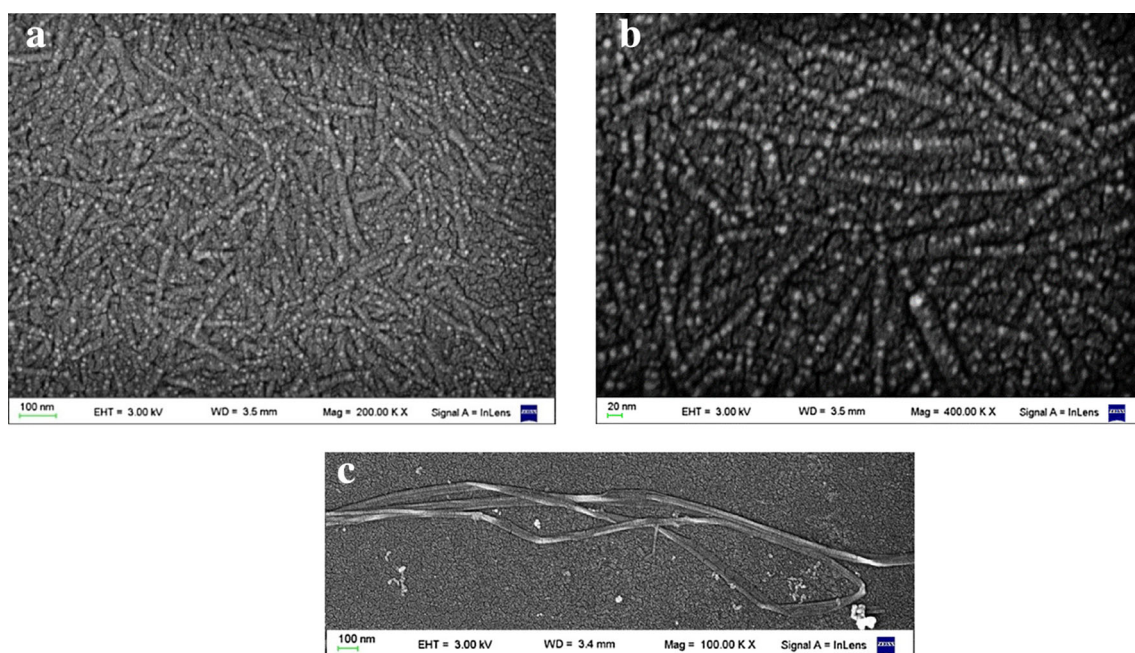


Fig. 3 SEM micrograph of CNC (a and b) and BC (c)

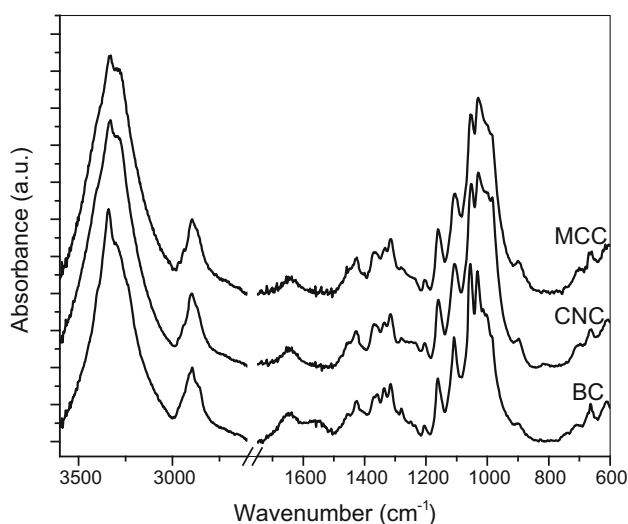


Fig. 4 FTIR spectra of MCC, CNC and BC

of cellulose I [28]. The crystallinity degree (X_c) was determined applying Eq. 1, and the values are presented in Table 1. CNC crystallinity was slightly higher than MCC, which confirms that the amorphous regions are more susceptible to acid treatment. Additionally, BC presented an intrinsic elevated crystallinity, according to that observed by FTIR.

Thermogravimetric Analysis

Thermal stability of CNC and BC was analyzed by TGA. Two weight loss stages below 400 °C were observed in the

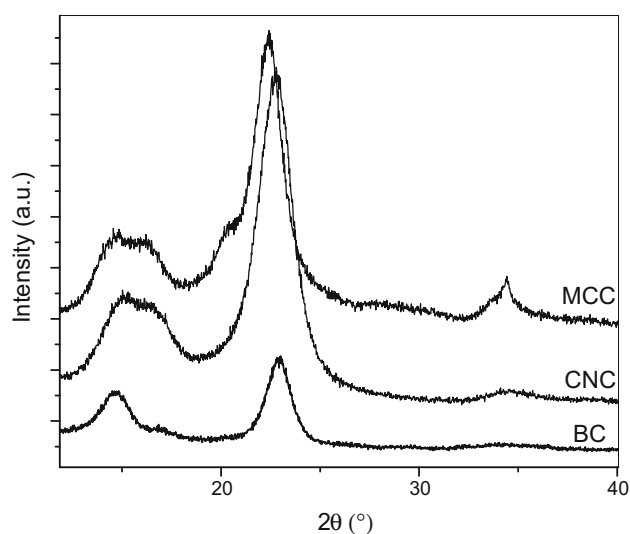


Fig. 5 DRX spectra of MCC, CNC and BC

first derivative of the weight loss curve with respect to temperature (DTG) curve of the samples (Fig. 6). The initial weight loss of approximately 3 % occurred around 100 °C (Fig. 6a), which correspond to the evaporation of physically adsorbed and hydrogen bond linked water molecules [13]. The second weight loss occurred between 100 and 400 °C (Fig. 6 b), and the corresponding temperature at the maximum degradation rate (T_d) and the weight loss at 400 °C of MCC, CNC and BC are reported in Table 1. A reduction of T_d was observed for CNC respect of MCC. When sulfuric acid is used as a hydrolyzing agent in CNC production, it reacts with the

Table 1 Degradation temperature and crystallinity degree of MCC, CNC and BC

Material	T _d (°C) (TGA)	Weight loss at 400 °C (%) (TGA)	X _c % (XRD)
MCC	336.2	94.21	71.7
CNC	299.8	74.90	72.7
BC	247.0–303.7	76.99	93.5

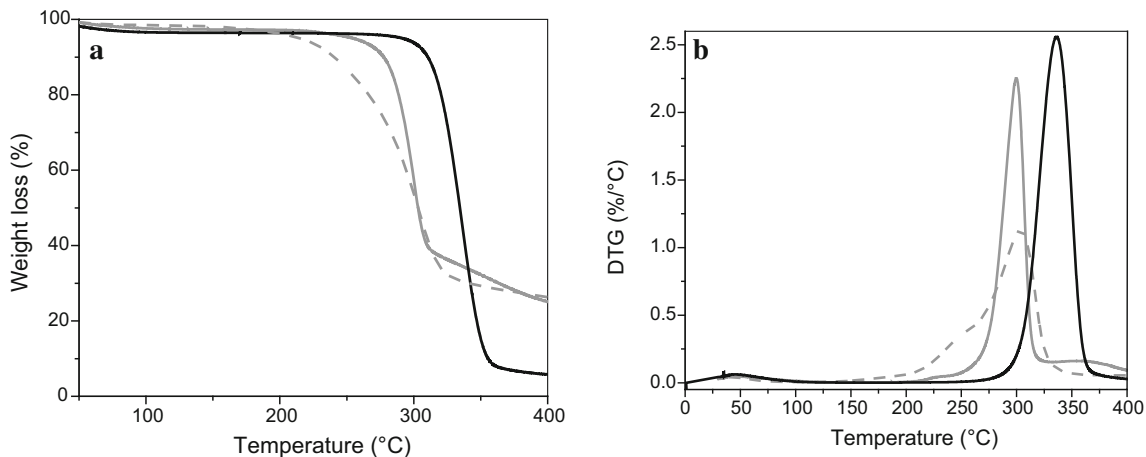


Fig. 6 Weight loss (a) and DTG (b) curves of: (black line) MCC, (grey line) CNC, (dashed line) BC

surface hydroxyl groups of cellulose to yield charged sulfate esters. The introduction of charged sulfate groups generates the reduction of the degradation activation energy and, subsequently, T_d decreases [29]. Roman and Winter [29] also observed that BC degrades between 200 and 400 °C. BC thermogram displayed two decomposition steps in the curve, starting its degradation at lower temperature than CNC or MCC. First stage could be due to the presence of bacterial cells unremoved, and the second corresponds to cellulose decomposition.

PHB Nanocomposites Characterization

Morphological Characterization

Nanoreinforced PHB with CNC and BC prepared by casting resulted in macroscopically homogenous and transparent films with a thickness ranging between 40 and 50 μm (Fig. 7). Different nanoparticles content were used: 2, 4 and 6 wt% of CNC and 2 wt% of BC.

SEM photographs of fractured sections of PHB and CNC/PHB nanocomposite films are shown in Fig. 8. It was observed that the cross-section of the pristine PHB was some rough and without cracks or pores. Comparatively, the cross-section of the CNC/PHB film was not strongly affected by the addition of CNC. The CNC were uniformly dispersed within the PHB matrix and the filler might be identified as white particles in the matrix

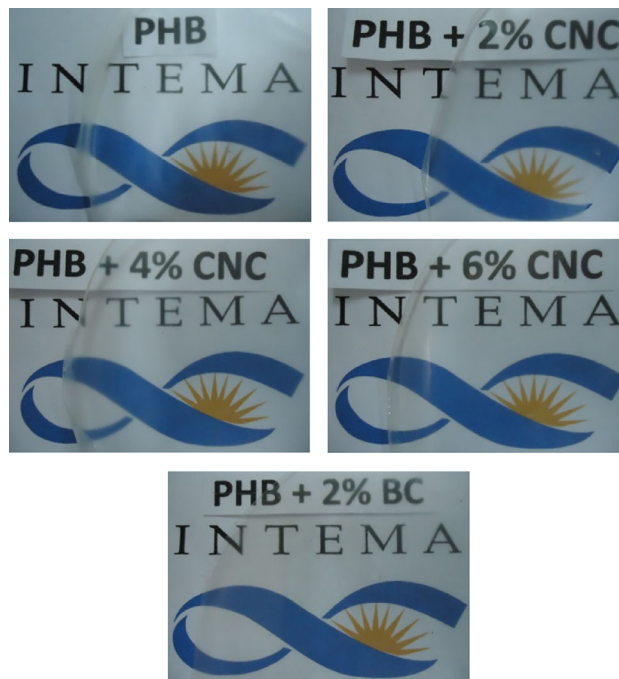
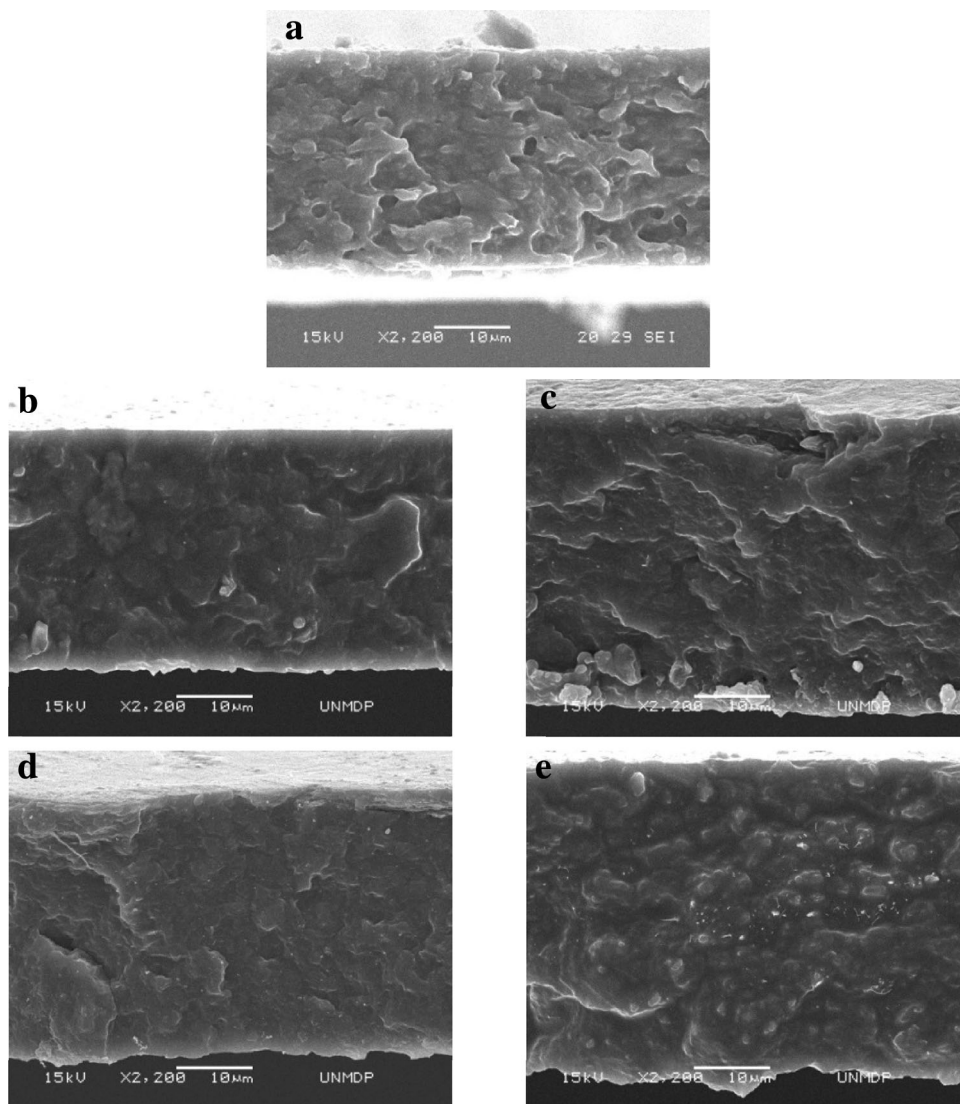


Fig. 7 Photography of films of PHB and their nanocomposites with CNC 2 wt%, CNC 4 wt%, CNC 6 wt%, BC 2 wt%

of PHB [30]. Regarding BC, it can be observed in Fig. 8e as white dots together with some white lines according with the longer length of the BC microfibrils compared to CNC.

Fig. 8 SEM of fractured surfaces of PHB (a), and their nanocomposites with CNC 2 wt% (b), CNC 4 wt% (c), CNC 6 wt% (d), BC 2 wt% (e)



Thermal and Structural Characterization

In order to study the melting and crystallization behavior as well as the morphology of PHB and their nanocomposites, DSC analyses were performed. Figure 9a shows the DSC traces of the first heating of casted PHB and their nanocomposites films and the thermal properties were summarized in Table 2. All DSC thermograms exhibited double melting behavior that can be explained by the melting, recrystallization and remelting model of PHB [31]. The lower temperature peak could be attributed to the melting of the original PHB crystals formed during the casting process (T_{m1}), while the higher one (T_{m2}) is due to crystals recrystallized during the DSC heating process [32]. Accordingly, melting temperature of PHB crystals (T_{m1}) are slightly shifted to higher temperatures in the nanocomposites, independently of the percentage of CNC added. This could indicate that the nanoparticles facilitated

PHB crystals growth leading to larger lamellar thickness or high ordered crystals in the spherulites during the casting process, which consequently displayed increased melting points. Additionally, PHB crystallinity obtained using Eq. 2, was similar regardless the percentage or type of nanoparticle added. On the other hand, the two types of nanoparticles studied act as nucleation agent of the PHB but without significantly change its percentage of crystallinity [33]. Moreover, the fusion temperature of the recrystallized crystals formed during the heating scan (T_{m2}) occurs at almost the same temperature regardless of the amount or type of nanoparticle added to the polymer. It was reported that the addition of CNC had no significant influence on T_m of the nanocomposites, no matter the nature of the matrix [30].

Figure 9b shows the DSC cooling scans of PHB and their nanocomposites obtained at a rate of 10 °C/min, after the first heating scan. Then, a second heating scan was

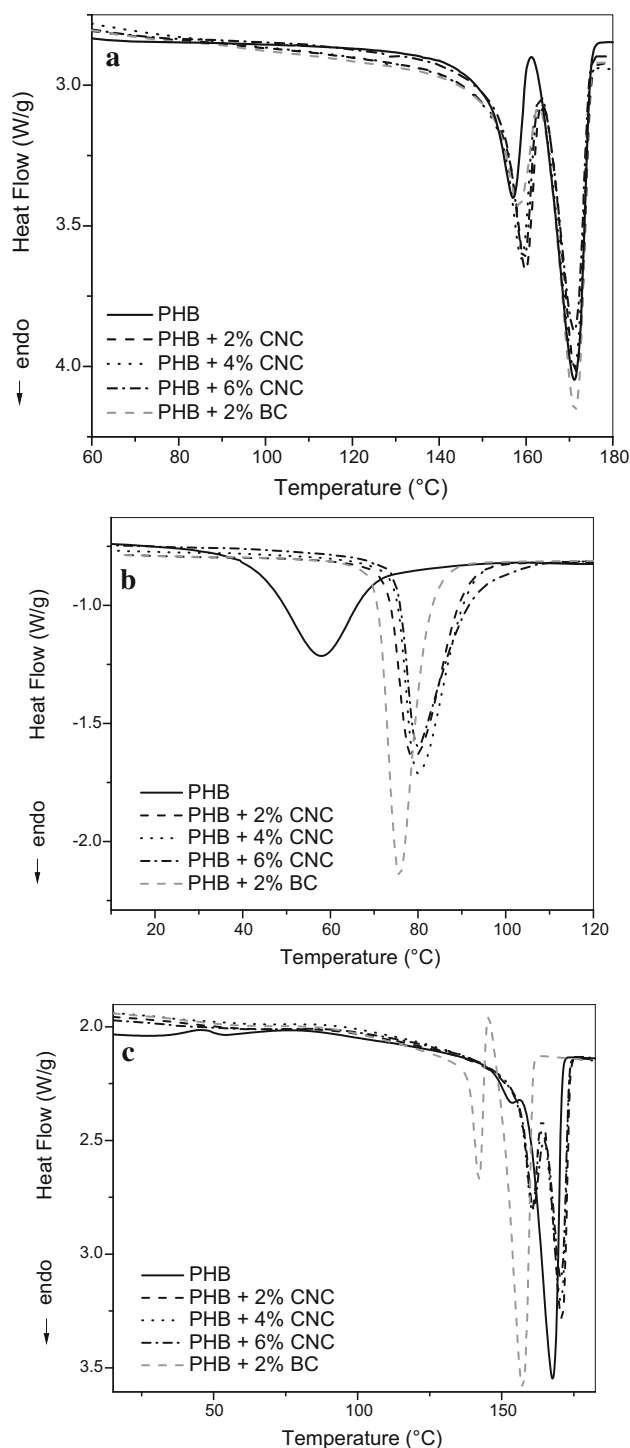


Fig. 9 DSC curves during first heating at 10 °C/min (a), cooling at 10 °C/min (b) and second heating at 10 °C/min (c) of PHB and nanocomposites

done on DSC in order to analyze the nanocomposites behavior after their thermal histories were erased (Fig. 9c). It was observed that a peak corresponding to the crystallization of PHB appears in all the samples during the

cooling process, but for nanocomposites it occurs before (at a higher temperature) than for the pristine PHB. This verifies that the nanofillers act as a nucleating agent of PHB. Many works had reported that cellulose nanoparticles could act as nucleating agents of different polymers [33–35].

Furthermore, in the second heating scan (Fig. 9c), a small crystallization peak together with a single melting peak with a small shoulder (T_{m1}) was detected for the pristine PHB. However, it was observed an increase in the area of the first melting peak for the nanocomposites compared to the single PHB. It appears that the crystals formed from the melt are more imperfect than that formed during the casting, process in which crystals have more time to form. Therefore, these crystals will recrystallize and reorganize into more perfect and stable crystals during the subsequent heating scans. Then, a greater relative area of T_{m2} than T_{m1} was induced in the second heating scan, compared to the first one [36]. In the case of BC the overall process occurs at lower temperature and an exotherm (the recrystallization peak) is observed between the two endotherms. The lower melting process could be attributed to a decrease in the degree of order of the crystals, due to the hindering effect of the BC which has higher aspect ratio than CNC.

XRD analyses were performed on PHB, CNC and their nanocomposites films. The XRD spectra of PHB and their nanocomposites are shown in Fig. 10a, b in order to analyze the effect of the nanoparticles in the crystalline structure of the PHB. The addition of CNC did not considerably modify the crystalline structure of PHB (Fig. 10a). However, changes in the shape of some peaks of the spectra with CNC addition were observed. The most affected PHB peaks were placed at 13.5°, 16.8° and 22.3°, attributed to (0 2 0), (1 1 0) and (1 1 1) planes, respectively [33]. These angles matched with typical CNC peaks located at 14.5°, 16° and 22.5° corresponding to (1 $\bar{1}$ 1), (1 1 0) and (2 0 0) planes, respectively. Moreover, the spectrum of the nanocomposite with BC (Fig. 10b) was more similar to that of the PHB. Then, BC addition did not modify the crystalline structure of the PHB.

In order to evaluate the effect of the incorporation of CNC on the thermal stability of PHB, dynamic thermal degradation measurements were done. Figure 11 shows the DTG curves of the PHB and their nanocomposites films. All the nanocomposites exhibited a single peak. In addition, it was observed that the addition of CNC slightly increases the temperature of the onset of thermal degradation (T_{onset}) and T_d of PHB. These are in accordance to the greater stability of CNC as regards to PHB and strong interactions between filler and matrix. As well as, the possibility of higher ordered PHB crystals in presence of

Table 2 Average values of melting temperatures (T_m), crystallinity degree (X_c), crystallinity index (CC) and glass transition temperature (T_g) of PHB and nanocomposites films

Material	1st heating DSC			2nd heating DSC			FTIR CC	DMA T_g (°C)
	T_{m1} (°C)	T_{m2} (°C)	X_c (%)	T_{m1} (°C)	T_{m2} (°C)	X_c (%)		
PHB	157.0	171.0	55.4	153.0	167.6	55.1	4.2	17.3
PHB + 2 wt% CNC	160.0	171.4	55.9	160.6	170.8	53.6	4.0	16.9
PHB + 4 wt% CNC	159.5	171.2	55.4	160.5	170.4	53.7	3.8	15.3
PHB + 6 wt% CNC	159.5	171.1	54.2	161.0	170.4	52.9	3.6	15.6
PHB + 2 wt% BC	157.8	170.9	55.5	142.2	157.3	52.0	3.9	15.6

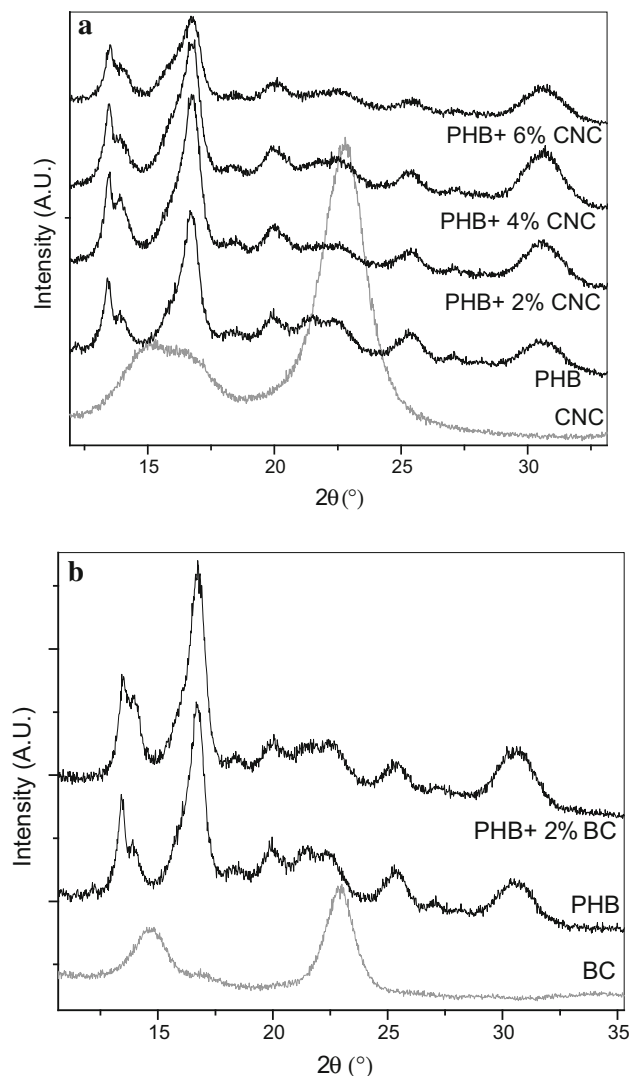


Fig. 10 **a** DRX spectra of PHB, CNC, PHB with 2, 4 and 6 wt% CNC. **b** DRX spectra of: PHB, BC and PHB with 2 wt% BC

CNC as it was observed in DSC could contribute to thermal stability enhancement [37]. All samples had less than 1 wt% residue at 400 °C and this value did not change with increasing CNC content.

Moreover, the addition of BC decreased the T_{onset} and T_d of PHB, reducing the thermal stability of the PHB. In this case the peak of PHB appears at approximately

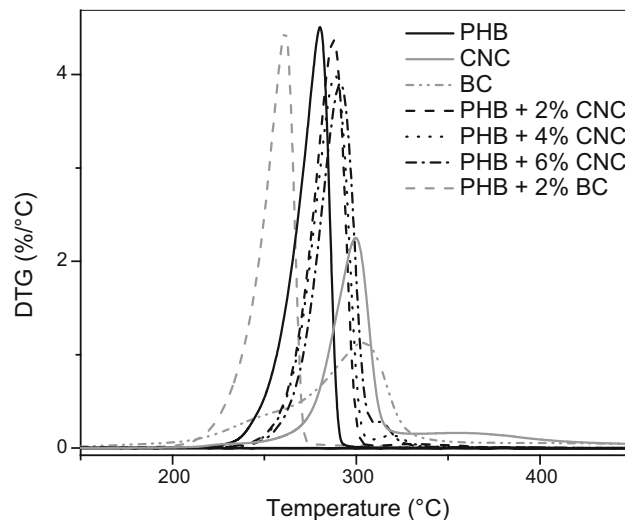
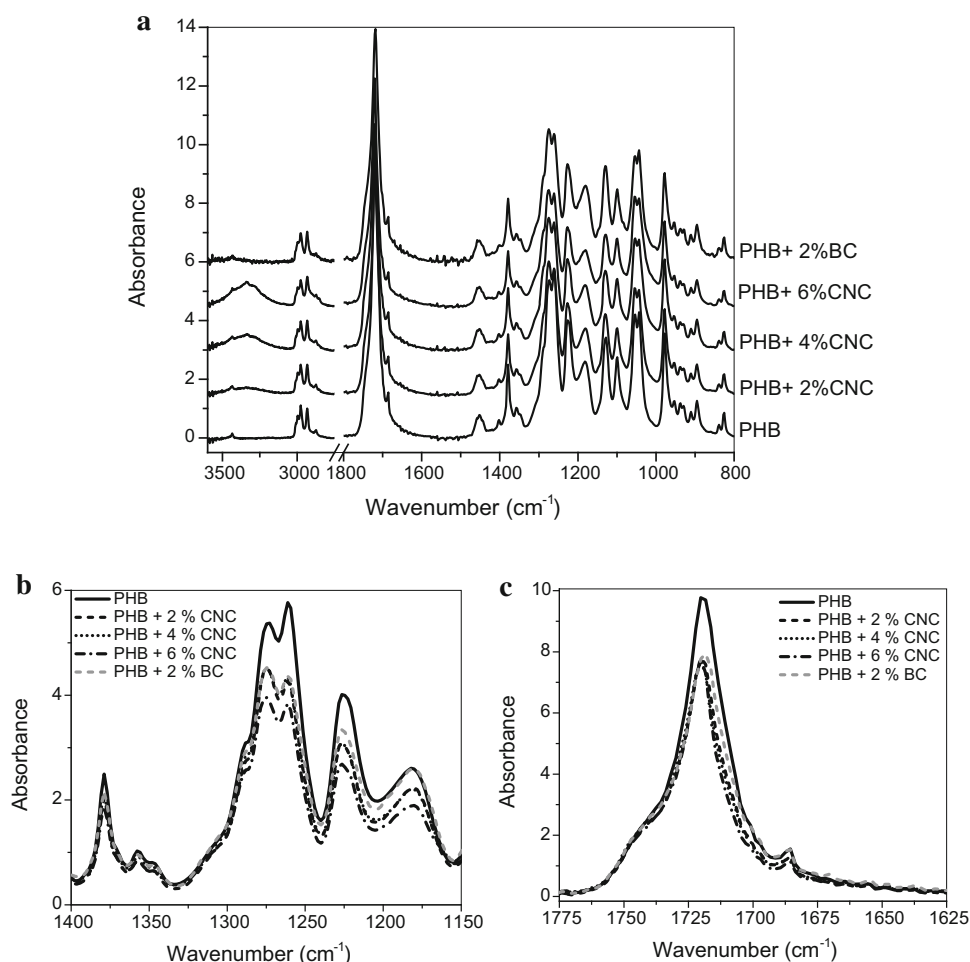


Fig. 11 DTGA curves of PHB, CNC, BC and nanocomposites

260 °C due to the less thermal stability of BC and worse dispersion of BC in the PHB nanocomposites. Then, BC cannot act as effective barrier to heat and volatiles compound diffusion.

FTIR spectra of the PHB and nanocomposite films were obtained (Fig. 12a) in order to study changes in the chemical structure of PHB in the nanocomposites. The spectra of PHB were not significantly modified by the addition of nanoparticles because of the high concentration of the polymer in the materials. A decrease of bands absorbance was observed in each composite spectra at 1720 cm^{-1} (C=O group of PHB) and at the range $1400\text{--}800\text{ cm}^{-1}$. The changes in the C=O bands with CNC addition could be due to the hydrogen interactions between the C=O groups of PHB and -OH groups of CNC [38, 39], as it was inferred by TGA. The multiple bands in the $1300\text{--}1100\text{ cm}^{-1}$ region (Fig. 12b) are due to the stretching of C–O–C groups in the crystalline (1276 and 1226 cm^{-1}) and amorphous phases (1261 and 1183 cm^{-1}) [40]. Additionally, Cyras et al. [23] defined a crystalline index (CC) as the ratio of the peak intensity at 1722 cm^{-1} to the intensity at 1740 cm^{-1} , which are related to C=O bond in the crystalline and the amorphous state, respectively (Fig. 12c). These peaks are overlapped and

Fig. 12 FTIR (ATR) spectra of lower surface films of PHB and nanocomposites (a), amplified characteristic regions of C–O–C (b) and C=O (c) bonds



deconvolution is required to establish precise intensities. It was observed that PHB crystallinity (Table 2) slightly decreased with the CNC or BC addition, indicating that the nanoparticles did not appreciably affect the crystallinity degree of PHB. Similar results were obtained for the X_c measured by DSC (Table 2). Moreover, the presence of CNC in the nanocomposites was observed in the 3500–3000 cm^{-1} region, characteristic of the –OH groups of cellulose structure, rising with increased CNC content in the nanocomposites. On the other hand, no modification of –OH band was perceived on BC nanocomposite spectrum, and it could be because of fewer interactions between matrix and BC caused by the morphology of BC.

Mechanical Properties

Uniaxial tensile tests were performed in order to determine the effect of cellulose nanoparticles on the PHB mechanical properties. The obtained Young's Modulus (E), tensile strength (σ_b) and elongation at break (ϵ_b) values are presented in Table 3. It can be seen that both E and σ_b of the CNC nanocomposites increased when compared to neat

PHB. The E of CNC nanocomposites increased by 60 %, σ_b increased 40 %, but ϵ_b decreased 25 %, independently of CNC content. Then, nanocomposites with different CNC content exhibited similar mechanical properties [14]. This behavior of nanocomposites could be due to the CNC dispersion achieved by sonication [17], and a possible formation of a percolating network of connecting particles through the nanocomposite film above a minimum filler amount, known as percolation threshold. It was reported that due to the high aspect ratio of CNC it has ability to set up 3D-percolating cellulose network structure interconnected by hydrogen bonding in matrix, standing for an improvement of the mechanical and barrier properties of polymers, once a good dispersion in matrix is achieved. As consequence, after this critical concentration there is no significant change in mechanical properties [25] and agglomeration is tended to form [17]. The agglomerations seem to act as defects or stress concentrations that result in a diminution of mechanical properties [17]. There is no appreciable improvement in mechanical properties of PHB with the incorporation of BC. In fact, BC nanocomposites presented worse mechanical properties than CNC

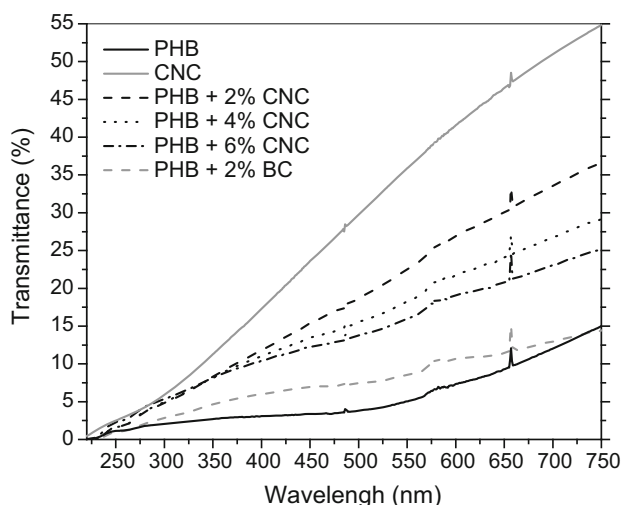
Table 3 Average values and corresponding error of tensile test results and WVP of PHB and nanocomposites films

Material	E (GPa)	σ_b (MPa)	ϵ_b	WVP. 10^{14} ($\text{g}\cdot\text{s}^{-1}\text{ m}^{-1}\text{ Pa}^{-1}$)
PHB	1.6 ± 0.2	20.5 ± 2.7	0.020 ± 0.004	159 ± 23
PHB + 2 wt% CNC	2.4 ± 0.3	29.7 ± 3.6	0.015 ± 0.002	133 ± 3
PHB + 4 wt% CNC	2.5 ± 0.2	29.2 ± 1.8	0.015 ± 0.002	107 ± 2
PHB + 6 wt% CNC	2.5 ± 0.2	30.5 ± 2.6	0.015 ± 0.002	94 ± 3
PHB + 2 wt% BC	1.8 ± 0.2	20.5 ± 3.2	0.012 ± 0.002	183 ± 23

nanocomposites. Higher aspect ratio of BC, in order of microns, reduces filler dispersion as it was observed by SEM, and the presence of agglomerations provokes the mechanical properties detrimental [8].

Transparency

Light protection is a basic requirement on packaging of food products and because of this, the development of a transparent material with enhanced UV protection is especially useful. Film transparency of nanocomposites was determined by UV–visible spectroscopy and the spectra are shown in Fig. 13. CNC film presented the highest UV–visible transmission. Nanocomposite films showed intermediate behavior between PHB and CNC films. At high energy range (220–400 nm) nanocomposites had low transmission, up to 10 %, in accordance with the reduce transmittance of the components at this radiation range. This result indicates that nanocomposites are better UV barrier than commodities polymers such as polypropylene, which presents 40–60 % of transmittance at the same radiation range [3].

**Fig. 13** Transmittance curves of PHB, CNC and nanocomposites films

Water Permeability

Finally, low vapor permeation is another requirement on food products packaging, and then the test was carried out to analyze the influence of CNC and BC in the PHB permeation. In Table 3 are shown the WVP values of PHB and nanocomposites films. An enhancement of moisture barrier property of nanocomposites due to the CNC addition was observed. It was probably due to an increment in the tortuosity of the vapor pathway, despite of the hydrophilic character of CNC. Different factors related to the filler influence this feature; such as quantity, shape, aspect ratio and orientation, dispersion degree, compatibility with matrix and crystallinity [41]. This result indicates that CNC have good dispersion and matrix interaction [42] as it was observed on permeation tests. While the nanocomposites with BC show an increase in permeation due to structure and length of microfibril adverse to generate a tortuous path for water vapor, in agreement with TGA observations.

Conclusions

Nanoreinforced PHB was obtained by solvent casting using different content of CNC and BC as fillers, resulting on macroscopically homogenous films.

Thermal properties of PHB and nanocomposites films were studied by DSC where the melting–recrystallization–remelting behavior of the casted PHB was observed. The crystalline structure and fusion temperature of PHB were not modified by the addition of the nanoparticles. Moreover, the two types of nanoparticles act as nucleating agents of PHB during the cooling DSC scan.

It was possible to improve the water vapor permeation, transparency, thermal and mechanical properties of PHB with the addition of low percentages of CNC due to the good dispersion and interaction of the filler with the polymeric matrix. Moreover, the PHB–BC nanocomposites did not show significant improvements in the material properties as PHB–CNC, due to the poorer dispersion and barrier capacity of the longest BC. Subsequently, the morphology, the aspect ratio and the structure of cellulose nanoparticles are very important aspects in improving the

properties of the matrix and play a significant role in these nanocomposites.

These results indicate that the PHB–CNC nanocomposites could be suitable materials to be used as packaging in certain applications. Whilst both CNC and BC serve as nano-reinforcement for the production of better performance materials than the PHB, but it was observed that CNC does outperform BC as reinforcement.

Acknowledgments The authors acknowledge the financial support of CONICET (PIP 0014 y 0527) y CNR-CONICET N° 1010, Agencia Nacional de Promoción Científica y Tecnológica (PICT'12 1983) and Universidad Nacional de Mar del Plata.

References

- Lucas N, Bienaime C, Belloy C et al (2008) Polymer biodegradation: mechanisms and estimation techniques—a review. *Chemosphere* 73:429–442. doi:10.1016/j.chemosphere.2008.06.064
- Savenkova L, Gercberga Z, Nikolaeva V et al (2000) Mechanical properties and biodegradation characteristics of PHB-based films. *Process Biochem* 35:573–579. doi:10.1016/S0032-9592(99)00107-7
- Bucci DZ, Tavares LBB, Sell I (2007) Biodegradation and physical evaluation of PHB packaging. *Polym Test* 26:908–915. doi:10.1016/j.polymertesting.2007.06.013
- Plackett D, Vázquez A (2004) Natural polymer sources. In: Baillie C (ed) *Green Compos*. Woodhead Publishing Limited, Cambridge, pp 123–153
- Sangkharak Kanokphorn (2011) Utilization of biodiesel waste as a feedstock for the production of polyhydroxybutyrate by *Cupriavidus necator*. *Afr J Biotechnol* 10:17812–17824. doi:10.5897/AJB11.2184
- Avella M, Martuscelli E, Raimo M (2000) Properties of blends and composites based on poly(3-hydroxy)butyrate (PHB) and poly(3-hydroxybutyrate-hydroxyvalerate) (PHBV) copolymers. *J Mater Sci* 35:523–545
- Erceg M, Kovačić T, Klarić I (2005) Thermal degradation of poly(3-hydroxybutyrate) plasticized with acetyl tributyl citrate. *Polym Degrad Stab* 90:313–318. doi:10.1016/j.polymdegradstab.2005.04.048
- Angelini S, Cerruti P, Immirzi B et al (2016) Acid-insoluble lignin and holocellulose from a lignocellulosic biowaste: bio-fillers in poly(3-hydroxybutyrate). *Eur Polym J* 76:63–76. doi:10.1016/j.eurpolymj.2016.01.024
- Wang S, Song C, Chen G et al (2005) Characteristics and biodegradation properties of poly(3-hydroxybutyrate-co-3-hydroxyvalerate)/organophilic montmorillonite (PHBV/OMMT) nanocomposite. *Polym Degrad Stab* 87:69–76. doi:10.1016/j.polymdegradstab.2004.07.008
- Díez-Pascual AM, Díez-Vicente AL (2014) Poly(3-hydroxybutyrate)/ZnO bionanocomposites with improved mechanical, barrier and antibacterial properties. *Int J Mol Sci* 15:10950–10973. doi:10.3390/ijms150610950
- de Carvalho KCC, Montoro SR, Cioffi MOH, Voorwald HJC (2016) Polyhydroxyalkanoates and their nanobiocomposites with cellulose nanocrystals. In: Thomas S, Shanks R, Chandrasekharakurup S (eds) *Des Appl. Nanostructured Polym. Blends Nanocomposite Syst*. Elsevier, Oxford, pp 261–285
- Siqueira G, Bras J, Dufresne A (2010) Cellulosic bionanocomposites: a review of preparation, properties and applications. *Polymers (Basel)* 2:728–765. doi:10.3390/polym2040728
- Hu W, Chen S, Yang J et al (2014) Functionalized bacterial cellulose derivatives and nanocomposites. *Carbohydr Polym* 101:1043–1060. doi:10.1016/j.carbpol.2013.09.102
- de Azeredo HMC (2009) Nanocomposites for food packaging applications. *Food Res Int* 42:1240–1253. doi:10.1016/j.foodres.2009.03.019
- Favier V, Cavaille JY, Canova GR, Shrivastava SC (1997) Mechanical percolation in cellulose whisker nanocomposites. *Polym Eng Sci* 37:1732–1739. doi:10.1002/pen.11821
- Moon RJ, Martini A, Nairn J et al (2011) Cellulose nanomaterials review: structure, properties and nanocomposites. *Chem Soc Rev* 40:3941–3994. doi:10.1039/c0cs00108b
- Cao Y, Zavattieri P, Youngblood J et al (2016) The relationship between cellulose nanocrystal dispersion and strength. *Constr Build Mater* 119:71–79. doi:10.1016/j.conbuildmat.2016.03.077
- Habibi Y, Lucia LA, Rojas OJ (2010) Cellulose nanocrystals: chemistry, self-assembly, and applications. *Chem Rev* 110:3479–3500. doi:10.1021/cr900339w
- Cherian BM, Leao AL, de Souza SF et al (2011) Cellulose nanocomposites for high-performance applications. In: Kalia S, Kaith BS, Kaur I (eds) *Cellulose fibers: bio- and nano-polymer composites*. Springer, Berlin, pp 539–587
- Dhar P, Bhardwaj U, Kumar A, Katiyar V (2015) Poly (3-hydroxybutyrate)/cellulose nanocrystal films for food packaging applications: barrier and migration studies. *Polym Eng Sci* 55:2388–2395. doi:10.1002/pen.24127
- Morán JI, Alvarez VA, Cyras VP, Vázquez A (2008) Extraction of cellulose and preparation of nanocellulose from sisal fibers. *Cellulose* 15:149–159. doi:10.1007/s10570-007-9145-9
- Vazquez A, Foresti ML, Cerrutti P, Galvagno M (2013) Bacterial cellulose from simple and low cost production media by *Gluconacetobacter xylinus*. *J Polym Environ* 21:545–554. doi:10.1007/s12192-010-0223-9
- Cyras VP, Galego Fernández N, Vázquez A (1999) Biodegradable films from PHB-8HV copolymers and polyalcohols blends: crystallinity, dynamic mechanical analysis and tensile properties. *Polym Int* 48:705–712
- Barham PJ, Keller A, Otun EL, Holmes PA (1984) Crystallization and morphology of a bacterial thermoplastic: poly-3-hydroxybutyrate. *J Mater Sci* 19:2781–2794. doi:10.1007/BF01026954
- Spence K, Habibi Y, Dufresne A (2011) Nanocellulose-based composites. In: Kalia S, Kaith BS, Kaur I (eds) *Cellulose fibers: bio- and nano-polymer composites*. Springer, Berlin, pp 179–213
- Oh SY, Il Yoo D, Shin Y et al (2005) Crystalline structure analysis of cellulose treated with sodium hydroxide and carbon dioxide by means of X-ray diffraction and FTIR spectroscopy. *Carbohydr Res* 340:2376–2391. doi:10.1016/j.carres.2005.08.007
- de Teixeira EM, Pasquini D, Curvelo AAS et al (2009) Cassava bagasse cellulose nanofibrils reinforced thermoplastic cassava starch. *Carbohydr Polym* 78:422–431. doi:10.1016/j.carbpol.2009.04.034
- Silvério HA, Flauzino Neto WP, Dantas NO, Pasquini D (2013) Extraction and characterization of cellulose nanocrystals from corncob for application as reinforcing agent in nanocomposites. *Ind Crops Prod* 44:427–436. doi:10.1016/j.indcrop.2012.10.014
- Roman M, Winter WT (2004) Effect of sulfate groups from sulfuric acid hydrolysis on the thermal degradation behavior of bacterial cellulose. *Biomacromolecules* 5:1671–1677. doi:10.1021/bm034519+
- Azizi Samir M, Alloin F, Dufresne A (2005) Review of recent research into cellulosic whisker, their properties and their application in nanocomposites field. *Biomacromolecules* 6:612–626
- Gunaratne LMWK, Shanks RA, Amarasinghe G (2004) Thermal history effects on crystallisation and melting of poly(3-hydroxybutyrate). *Thermochim Acta* 423:127–135. doi:10.1016/j.tca.2004.05.003

32. Pearce R, Marchessault R (1994) Multiple melting in blends of isotactic and atactic poly(β -hydroxybutyrate). *Polymer (Guildf)* 35:3990–3997. doi:[10.1016/0032-3861\(94\)90285-2](https://doi.org/10.1016/0032-3861(94)90285-2)
33. Ten E, Jiang L, Wolcott MP (2012) Crystallization kinetics of poly(3-hydroxybutyrate-co-3-hydroxyvalerate)/cellulose nanowhiskers composites. *Carbohydr Polym* 90:541–550. doi:[10.1016/j.carbpol.2012.05.076](https://doi.org/10.1016/j.carbpol.2012.05.076)
34. Simonsen J, Habibi Y (2009) Cellulose nanocrystals in polymer matrices. In: *The nanoscience and technology of renewable biomaterials*. Wiley, Chichester, pp 273–292
35. Frone AN, Berlioz S, Chailan JF, Panaitescu DM (2013) Morphology and thermal properties of PLA-cellulose nanofibers composites. *Carbohydr Polym* 91:377–384. doi:[10.1016/j.carbpol.2012.08.054](https://doi.org/10.1016/j.carbpol.2012.08.054)
36. Xu C, Qiu Z (2009) Nonisothermal melt crystallization and subsequent melting behavior of biodegradable poly(hydroxybutyrate)/multiwalled carbon nanotubes nanocomposites. *J Polym Sci Part B Polym Phys* 47:2238–2246. doi:[10.1002/polb.21821](https://doi.org/10.1002/polb.21821)
37. Fortunati E, Armentano I, Zhou Q et al (2012) Multifunctional bionanocomposite films of poly(lactic acid), cellulose nanocrystals and silver nanoparticles. *Carbohydr Polym* 87:1596–1605. doi:[10.1016/j.carbpol.2011.09.066](https://doi.org/10.1016/j.carbpol.2011.09.066)
38. Zhang J, Sato H, Noda I, Ozaki Y (2005) Conformation rearrangement and molecular dynamics of poly(3-hydroxybutyrate) during the melt-crystallization process investigated by infrared and two-dimensional infrared correlation spectroscopy. *Macromolecules* 38:4274–4281. doi:[10.1021/ma0501343](https://doi.org/10.1021/ma0501343)
39. Mottin AC, Ayres E, Eliane A et al (2016) What changes in poly(3-hydroxybutyrate) (PHB) when processed as electrospun nanofibers or thermo-compression molded film? *Mater Res* 19:57–66
40. de O Patrício PS, Pereira FV, dos Santos MC et al (2013) Increasing the elongation at break of polyhydroxybutyrate biopolymer: effect of cellulose nanowhiskers on mechanical and thermal properties. *J Appl Polym Sci* 127:3613–3621. doi:[10.1002/app.37811](https://doi.org/10.1002/app.37811)
41. Fortunati E, Peltzer M, Armentano I et al (2012) Effects of modified cellulose nanocrystals on the barrier and migration properties of PLA nano-biocomposites. *Carbohydr Polym* 90:948–956. doi:[10.1016/j.carbpol.2012.06.025](https://doi.org/10.1016/j.carbpol.2012.06.025)
42. Avérous L, Pollet E (2012) Green Nano-Biocomposites. In: Avérous L, Pollet E (eds) *Environmental silicate nano-biocomposites*. Springer, London, pp 1–11